

PAPER

Charge exchange recombination spectra for 100 keV/u and 500 keV/u atomic hydrogen beam colliding with W^{64+}

Recent citations

- [Atomic Data for Calculation of the Intensities of Stark Components of Excited Hydrogen Atoms in Fusion Plasmas](#)
Oleksandr Marchuk *et al*

To cite this article: Yu Ralchenko and D R Schultz 2019 *Plasma Phys. Control. Fusion* **61** 125007

View the [article online](#) for updates and enhancements.



IOP | ebooks™

Bringing together innovative digital publishing with leading authors from the global scientific community.

Start exploring the collection—download the first chapter of every title for free.

Charge exchange recombination spectra for 100 keV/u and 500 keV/u atomic hydrogen beam colliding with W^{64+}

Yu Ralchenko¹  and D R Schultz^{2,3}

¹ Atomic Spectroscopy Group, National Institute of Standards and Technology, Gaithersburg, MD 20899-8422, United States of America

² Department of Physics, University of North Texas, Denton, TX 76203, United States of America

E-mail: yuri.ralchenko@nist.gov

Received 17 July 2019, revised 26 September 2019

Accepted for publication 11 October 2019

Published 28 October 2019



CrossMark

Abstract

We present synthetic spectra for light emission following charge exchange (CX) recombination for Ne-like W^{64+} ions colliding with neutral atomic hydrogen at 100 and 500 keV/u, which is of relevance to the plasma diagnostics of the international experimental fusion device ITER now under construction. The spectra are calculated using a detailed collisional-radiative model for the W^{63+} ion that includes more than 6000 singly- and doubly-excited states and accounts for major physical processes in hot fusion plasmas. The CX cross sections into excited states are computed using the classical trajectory Monte Carlo method. A comprehensive analysis of the modifications to the spectra due to CX is presented.

Keywords: neutral beams, charge exchange, ITER, tungsten, collisional-radiative modeling, classical trajectory Monte Carlo

(Some figures may appear in colour only in the online journal)

1. Introduction

Charge exchange recombination spectroscopy (CXRS, or CHERS) [1–4] is an important diagnostic technique used in fusion energy research to determine certain plasma properties such as its rotation velocity. It requires, as its name implies, knowledge of the charge transfer process involved in the collision of the highly charged ions that are either intrinsic to these plasmas (for example, being sputtered from the confinement vessel and then stripped to high charge states in the core plasma) or have been introduced intentionally (such as species that can act as tracers, radiative coolants, or for other purposes). The charge exchange occurs between these highly charged ions and atomic hydrogen introduced through high-energy neutral beam injection, either for diagnostic purposes or, most often, to heat the plasma allowing the diagnostic to proceed parasitically. When the highly charged ion captures

one or more electrons from the atoms of the neutral beam, it occurs predominantly to large principal quantum number, resulting in radiative de-excitation yielding photons in various spectral ranges. Detection and analysis of the resulting spectrum then allows determination of characteristics of the plasma.

Since the preeminent fusion experiment of the next twenty years will be the ITER device presently under construction by an international collaboration in France [5], it is important to develop early on the required base of knowledge for CXRS. Recently we undertook calculation of a large database of state-selective charge transfer for Ar^{q+} ($q = 15–18$) colliding with atomic hydrogen [6] over a wide range of energies relevant to ITER neutral beam injection (and lower energies relevant to ongoing plasma experiments [7]). Such noble gases are introduced for diagnostics purposes, to enhance radiative cooling of the plasma, or to mitigate plasma disruptions. Here, we report similar calculations for $W^{64+} + H(1s)$ at ITER neutral beam relevant energies, as well as predictions of the resulting spectra of

³ Present address: Department of Physics and Astronomy, Northern Arizona University, Flagstaff, AZ 86011, United States of America.

photons emitted through direct and cascade de-excitation following the charge transfer. This element will be intrinsic to ITER, for which most of the plasma-facing surface of the divertor will be made of tungsten, and W^{64+} is expected to be the most abundant ion in the core plasma of ITER. The future ITER neutral beams will make use of hydrogen and deuterium. The present work only addresses the H beam and the D beam interactions with W will be analyzed elsewhere. This is the first detailed computation of charge exchange recombination for such highly-charged ions of tungsten.

2. Collisional calculations

A simple model predicting the principal quantum number for the predominant charge transfer probability described by Olson [8] indicates that the electron tends to maintain a balance of both its initial orbital energy and orbital dimensions in the transition from the target state to the projectile state. This model, and results of other theoretical methods (see e.g. [9]), show that $n_{\max} \approx q^{3/4}$. For a charge state, q , of 64, $n_{\max} \approx 23$. In addition, it is known that above n_{\max} the n -resolved charge transfer cross section eventually falls off as $1/n^3$, indicating that the cross section is a significant fraction of its value at n_{\max} for n 's in the range of 30, 40, or more. Few theoretical methods are capable of treating charge transfer in ion-atom collisions to large principal quantum numbers and, as far we are aware, only one is capable of doing so for the very large n levels relevant for $W^{64+} + H$, namely, the classical trajectory Monte Carlo (CTMC) method [10, 11].

In brief, the CTMC method simulates the ion-atom collision through consideration of a large ensemble of trajectories that are chosen from an initial ensemble of configurations of the projectile—target system, chosen in such a way as to mimic as closely as possible the actual quantum mechanical distributions of electronic momentum and position. The classical mechanical equations of motion are then solved in time for the subsequent motion of, in this case, the three particles—projectile ion treated as a bare charge (the most tightly bound electrons being assumed to be inert since the capture proceeds to much higher n levels), the target proton of the hydrogen atom, and the target electron. At an asymptotic, final separation of the projectile and target, the relative energies of the particles are calculated in order to determine if a transition has occurred, that is, whether ionization, charge transfer, or excitation has taken place. If charge transfer has occurred, then the classical orbital state can be mapped following rules [12] that make a correspondence with quantum state principal and angular momentum quantum numbers. Large datasets of state-selective charge transfer cross sections have been computed for use in CXRS using CTMC, for example, for C^{6+} and O^{8+} [13], He^{2+} [14, 15], Ne^{q+} ($q = 7-10$) [16], Be^{q+} ($q = 2-4$) [17, 18], and as noted above, Ar^{q+} ($q = 15-18$) [6, 7] colliding with atomic hydrogen, and compared and validated where possible with theoretical results from quantum mechanical methods in overlapping regimes of applicability and with the limited measurements available.

There have been two principal variants of the CTMC method as applicable to one-electron systems such as present case in which the electrons on the W^{64+} projectile are considered inactive, namely, (i) CTMC utilizing a microcanonical distribution of orbits [10, 11] and (ii) a variation called 'rCTMC' based on using an alternative phase space distribution of initial orbits [19, 20]. The former is the original and most frequently employed variant. We denote this model 'pCTMC' here to clearly distinguish it, the 'p' standing for 'momentum' because the choice of the microcanonical distribution (i.e. $\delta(\mathcal{H} - E) = 0$, where \mathcal{H} is the target atom Hamiltonian and E the initial binding energy, -0.5 atomic units (a.u.)) reproduces exactly the quantum mechanical electronic momentum probability distribution. In contrast, rCTMC, developed in order to mimic closely the quantum mechanical electronic radial distribution, uses a non-sharp distribution of initial orbital energies. For example, Hardie and Olson [19] adopted a set of several microcanonical distributions with different initial binding energies to achieve this while Cohen [20] devised a continuous function of E that dictated the resulting ensemble of orbitals. Recently, a third variant, referred to as 'ZCTMC', has been introduced [21] that uses a non-sharp nuclear charge, Z , rather than non-sharp binding energy, to make the electronic radial distribution mimic the quantum mechanical results as rCTMC does.

The supposed advantage of the rCTMC approach is the allowance of orbits with radii larger than the classical cut-off that result from the microcanonical distribution, without substantially worsening the momentum distribution. The 'price to pay' by adopting the rCTMC approach is a non-sharp initial energy distribution of orbits, that is, the orbits will not all have the H(1s) binding energy of -0.5 a.u. Beyond the theoretical aesthetics of the pCTMC or rCTMC, the utility of either approach can be judged by comparison with robust quantum mechanical approaches or with measurements.

For the presently considered highly-charged ion, we are unaware of direct experimental measurements for comparison. Two works have sought to compare these models with results of quantum mechanical treatments for the highly charged ion Ar^{17+} colliding with atomic hydrogen, motivated in large part by the needs of CXRS. One of these used the conventional approach, pCTMC, to treat 13.333–250 keV/u $Ar^{q+} + H(1s, 2s, 2p)$ ($q = 15-18$) [6] in order to provide a comprehensive database of state-selective charge transfer cross sections required for Ar CXRS, and extended previous work [22]. That work used a method known as atomic-orbital close-coupling (AOCC) (see, e.g. the review by Fritsch and Lin [23]) that is a solution of the time-dependent Schrödinger equation (TDSE) in which the wavefunction is expanded in atomic states centered on the target and projectile. It was found that results of the AOCC method supported the pCTMC results obtained. In contrast, Errea *et al* [24] adopted the rCTMC approach to treat 20–300 keV/u $Ar^{q+} + H(1s)$ ($q = 16-18$) and found agreement with their molecular-orbital close-coupling (MOCC) results (see, [24, 25]).

Obtaining well converged, numerically accurate and stable solution of the TDSE in either the AOCC or MOCC

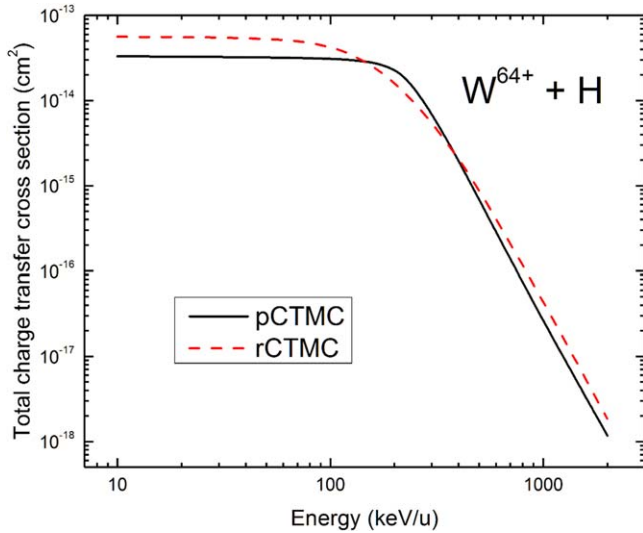


Figure 1. Comparison of the total cross section for charge transfer in collisions of W^{64+} with atomic hydrogen across wide impact energy range calculated via the two applicable variants of the CTMC method.

approach is a significant challenge for highly charged ions and high principal quantum numbers and therefore the disagreement between these two advanced methods is perhaps not surprising. In the present case, instead of n_{\max} of approximately 8 or 9 for the argon ions of interest, we have $n_{\max} \approx 23$ for $W^{64+} + H(1s)$ exacerbating these difficulties greatly. In particular, to seek confirmation of one or the other CTMC approach from a quantum mechanical method, we attempted to repeat our AOCC calculations as performed for $Ar^{18+} + H(1s)$ [6] but were unable numerically to obtain the required basis states for W^{63+} much less stable and convergent numerical solution of the TDSE. We also tried to no avail to use another standard approach for state-selective charge transfer calculations, applicable in the high impact energy regime, namely, the continuum distorted-wave method in perturbation theory ([25] and references therein), encountering numerical difficulties in producing states at high principal quantum number.

Therefore, in the present work, we have computed results using both pCTMC and rCTMC. Fortunately, as described below, for ITER-relevant impact energies, results of the two approaches do not differ nearly as much as they do for low-impact energy.

2.1. State-selective charge transfer cross sections

It is useful to first display the total cross section for charge transfer, obtained with both pCTMC and rCTMC, in order to see the general magnitude of the cross section across a broad range of impact energies, and to note the differences between results of the two approaches. As shown in figure 1, both methods give the same general behavior, with a plateau of the cross section below approximately 200 keV/u and then a sharp fall off at higher energies. At the beam energies discussed in the present work (i.e. 100 and 500 keV/u), as well as at 1 MeV/u that is also discussed as a possible energy for

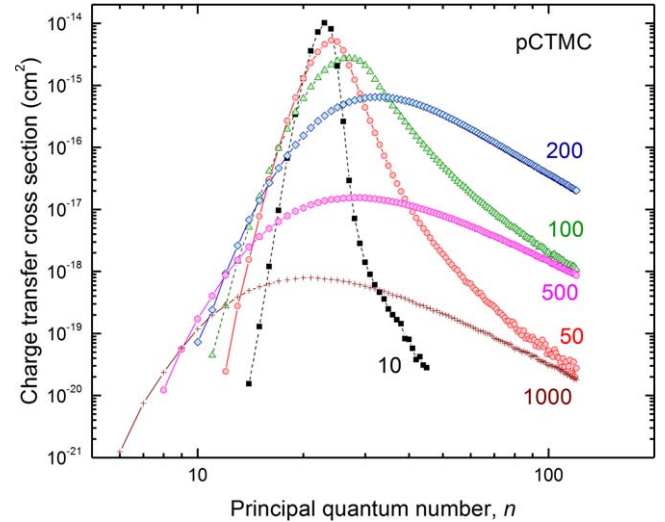


Figure 2. The n -resolved state-selective charge transfer cross section given by the pCTMC approach for several impact energies (at keV/u).

the ITER heating beam, the difference between integral cross sections predicted by the two methods is approximately 35%.

The behavior of the n -resolved state-selective charge transfer cross section for different projectile energies given by the pCTMC method is presented in figure 2. The width of the distribution significantly widens with increasing impact energy, and the n level with the greatest cross section is roughly approximated by the formula $n_{\max} = q^{3/4}$ (here equal to 23) but varies significantly as a function of impact energy, with $n_{\max} = 23, 24, 27, 33, 29,$ and 21 for 10, 50, 100, 200, 500, and 1000 keV/u, respectively.

As might well be expected, the n -resolved state selective charge transfer cross sections from the rCTMC model differ from those computed using pCTMC, as illustrated in figure 3. This is a particularly strong variation for the lowest impact energies, for example, 10 keV/u, where the n -distribution from rCTMC is on the order of three times as broad in n as that from pCTMC. At higher energies, for example those relevant to ITER neutral beam CXRS (i.e. about 500 keV/u), rCTMC differs less from pCTMC. This comes about because the charge transfer process becomes more dependent on matching the initial orbital velocity with the projectile velocity as impact energy increases and the pCTMC and rCTMC initial electronic momentum distributions differ much less than the corresponding electronic radial distributions.

Even so, by 100 keV/u, the n -resolved cross sections still differ significantly, as seen in figure 4 where the results of the two approaches are compared in an enlarged view. Also shown there is the well-known $1/n^3$ scaling of the n -dependence of the cross section, indicating that this behavior has an earlier onset in the rCTMC results (at about $n = 50$) than in the pCTMC results (at about $n = 100$).

The n - and ℓ -resolved cross sections for charge transfer are shown in figure 5 for 100 keV/u, and display characteristics common to all impact energies considered, consistent with those first described by Olson's pCTMC calculations of state-selective charge transfer in multiply-charged ion impact

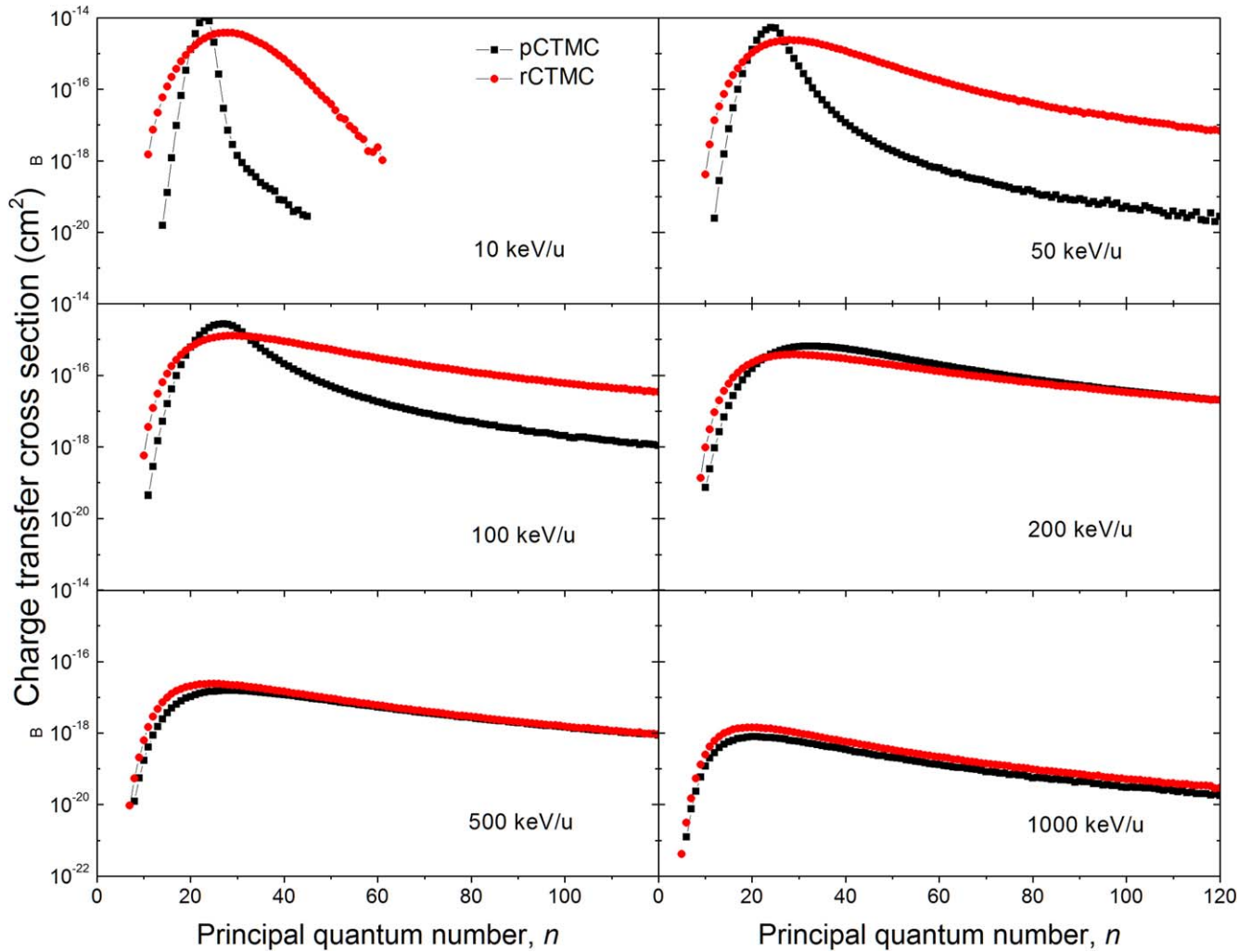


Figure 3. Comparison of pCTMC and rCTMC results for the n -resolved state selective charge transfer cross section at several energies.

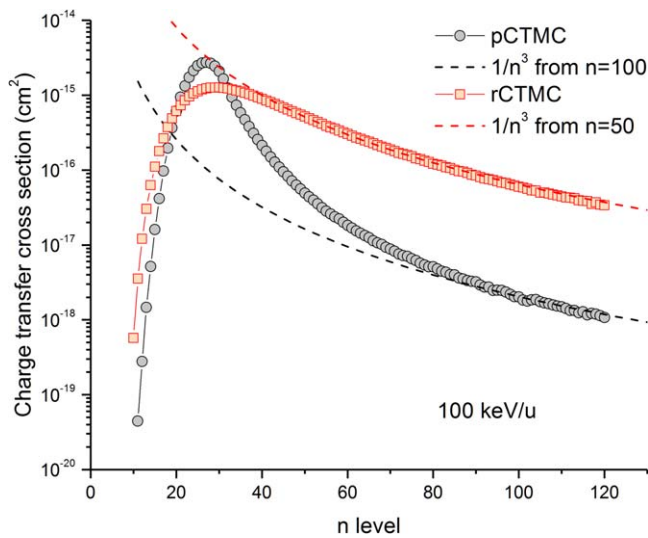


Figure 4. Comparison of pCTMC and rCTMC n -resolved charge transfer cross sections for 100 keV/u $H + W^{6++}$ with the well-known Wigner $1/n^3$ scaling with large n .

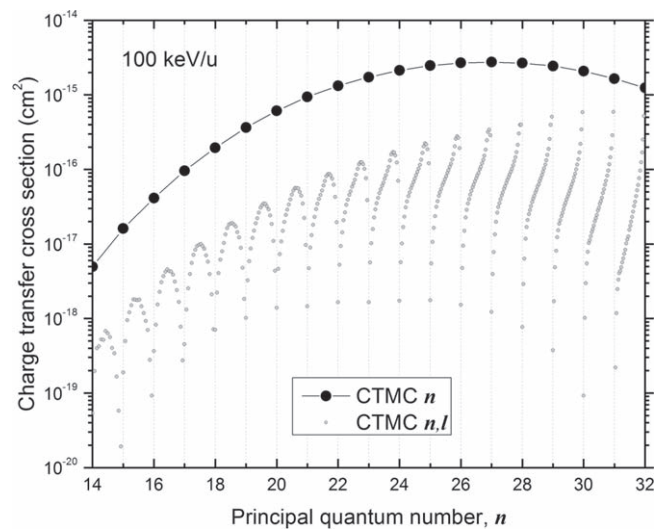


Figure 5. The n - and l -resolved state selective charge transfer cross section for 100 keV/u $W^{6++} + H$. The l -resolved cross sections for each n are plotted at abscissas given by $n + l/n$ for ease of display.

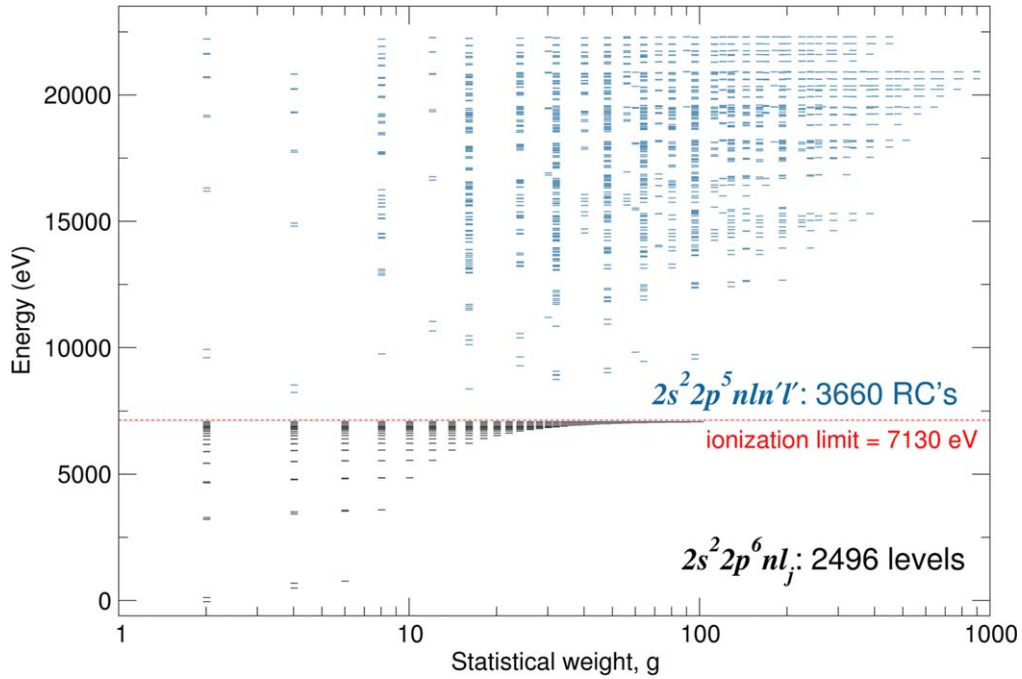


Figure 6. Energy structure of the W^{63+} ion as implemented in the collisional-radiative model. The atomic states below the ionization limit are represented by levels while those above by relativistic configurations.

of H [8]. That is, for $n < n_{\max}$ the cross sections as a function of the orbital angular momentum quantum number are more highly peaked than statistical towards large ℓ values, while for $n > n_{\max}$ they maximize around $\ell = q^{3/4}$. This occurs because the low n -level populations come about primarily from small impact parameter collisions in which an electron with high orbital angular momentum from the initial ensemble of orbits is captured from a tight, nearly circular orbit. For large n -levels, electrons with large classical eccentricities, and therefore low angular momenta, are captured preferentially in large impact parameter collisions. Therefore, processes that preserve the electron's orbital angular momentum are more probable.

3. Collisional-radiative simulations for post-CX spectra

3.1. Model description

In the $T_e \approx 20$ keV plasma of the ITER core the tungsten ionization distribution is peaked near the closed-shell Ne-like ion W^{64+} . This follows from, for example, a detailed comparison of calculations performed with advanced collisional-radiative (CR) codes at the NLTE Code Comparison Workshops [26]. The fact that the maximum abundance is reached for the ion with the ionization energy I smaller than the electron temperature seems contradictory to the well-known empirical formula $I \approx (0.1-0.3)T_e$ [27]. This rule, however, is typical for low- to mid-Z ions while for high-Z ions a different behavior $I \gtrsim T_e$ is expected [26].

Below we will only consider the charge transfer from Ne-like W^{64+} into Na-like W^{63+} . The 20 keV tokamak plasma

contains a number of significantly populated ions of tungsten and hence any realistic calculation of CX effect on plasma spectra should be carried out with a multi-ion CR model [28]. Nonetheless, the present simulation allows one to perform the most comprehensive and detailed analysis of the resulting CX spectra. An extensive analysis of complete CX spectra with a realistic ionization distribution including the most populated ions of W under the ITER core conditions will be published elsewhere.

For the CR simulations reported below we make use of the code NOMAD [29] that has been widely utilized for simulation of emission from laser-produced, astrophysical and magnetic confinement fusion plasmas. The present CR model includes (i) the ground state $2s^2 2p^6$ for the Ne-like ion and (ii) 2496 $2s^2 2p^6 nl_j$ fine-structure levels with $3 \leq n \leq 50$ ($l = 0..n-1$) as well as 3660 autoionizing states represented by relativistic configurations (RC) $2p^5 \underline{n}l'n'l'$ with $3 \leq n, n' \leq 8$ for the Na-like ion. Figure 6 provides a visual representation of the energy density of the included atomic levels and RCs and their statistical weights, illustrating that the model is very extensive. The excited states in W^{64+} can be safely ignored for the present study since their population is much smaller than that of the ground state and thus they do not contribute to the charge exchange population flux into the Na-like ion. The energies of the states included were calculated with the relativistic-model-potential flexible atomic code (FAC) [30], which is known to provide good accuracy for atomic structure and collision parameters of highly-charged ions. FAC was also used to calculate the radiative transition probabilities between all states including forbidden transitions of higher multipoles, autoionization rates and dielectronic capture cross sections, the electron-impact ionization cross sections, and the radiative recombination cross sections. The

electron-impact excitation cross sections were calculated in two approximations. For transitions between singly-excited states with $n \leq 8$ the distorted-wave method of FAC was used. For all other transitions we made use of the van Regemorter method using the FAC oscillator strengths. The latter were also used to account for proton-impact excitation cross sections with $\Delta n = 0$ that are particularly important for collisional redistribution of populations for high- n levels.

The choice to limit the highest level included in the model to be $n = 50$ for singly-excited $2s^2 2p^6 nl$ levels has been made for several reasons. Figures 2–5 show that the CTMC calculations were performed up to a much higher values of $n = 120$. Nevertheless, a detailed CR model extending up to such high values of the principal quantum number would be hardly manageable with the available computational resources. In fact, the limitation to $n \leq 50$ in the model provides a reasonable representation of population kinetics for CX case: for both (100 and 500 keV/u) rCTMC calculations as well as the pCTMC case at 500 keV/u the levels with $n \leq 50$ account for more than 2/3 of the total CX population flux, and for the 100 keV/u pCTMC case more than 98% of the CX cross section is accumulated for $n \leq 50$.

It should also be mentioned that our model only includes CX originating from the H ground state $1s$. Although the metastable state $2s$ in the beam may be well populated during beam production, after entering the strong magnetic field of a tokamak it will be immediately Stark mixed with the $2p$ state due to the induced electric field and decay radiatively over the first few centimeters [31].

3.2. Ionization balance shift

In a steady-state plasma of tokamaks the ionization balance for tungsten ions is primarily established through competition between electron-impact ionization and radiative and dielectronic recombination. Plasma transport may also affect ionization distributions but for the present paper that addresses only the most basic atomic processes this plasma effect is neglected. The three-body recombination is completely negligible due to a low plasma density, and heavy particle (proton) collisions for ion-charge-changing processes have much lower rates than electron interactions. Under these conditions, the ratio of ion populations between two neighboring states, here for W^{63+} and W^{64+} , is:

$$\frac{N_{64}}{N_{63}} = \frac{R_I}{R_{RR} + R_{DR}} \quad (1)$$

with R_I , R_{RR} and R_{DR} being the total rates of ionization, radiative recombination, and dielectronic recombination, respectively. The comparisons of total ionization and recombination rates at $T_e = 20$ keV and $n_e = 10^{14} \text{ cm}^{-3}$ performed at the NLTE-6 Code Comparison Workshop show that $R_I \approx 1000 \text{ s}^{-1}$ and $R_{RR} + R_{DR} \approx 650 \text{ s}^{-1}$ so that $N_{64} \approx 1.54 \times N_{63}$.

Injection of a neutral beam introduces an additional and very strong recombination channel due to charge exchange which appears as the additional term R_{CX} in the denominator of the rhs of equation (1). A simple estimate of the total CX

rate can be given as:

$$R_{CX} = n_0 \sigma_{CX}(E) v, \quad (2)$$

where n_0 is the density of neutrals in the beam, σ_{CX} is the total CX cross section at energy E , and v is the relative velocity between the beam particles and the W ions. For the 100 keV diagnostic beam for ITER, the product $n_0 v$ is about $2 \times 10^{17} \text{ cm}^{-2} \text{ s}^{-1}$. Taking $\sigma_{CX} \approx 3 \times 10^{-14} \text{ cm}^2$ from figure 1 at 100 keV/u, we obtain $R_{CX} \approx 3000 \text{ s}^{-1}$ which is much larger than the total recombination rate. However, since the neutrals do not occupy the whole volume of tokamak plasma, the CX contribution should be rescaled by the ratio of the beam volume V_B to the whole torus volume V_T [4]. This simplified picture clearly ignores the attenuation of the beam in plasma but nonetheless, it should provide a reasonable qualitative estimate. Thus, assuming the cross section of the neutral beam of 0.5 m^2 and the length of the beam propagation inside the torus of 6 m, the ratio V_B/V_T becomes about 0.0036 for ITER volume of 840 m^3 . Therefore, the additional effective recombination rate for the *averaged plasma volume* is only about 10 s^{-1} which thus is insufficient to noticeably modify the ionization balance of W. Again, it has to be emphasized that accurate quantitative considerations as to the importance and effect of charge exchange on ionization balance and level populations should be derived from time-dependent collisional-radiative simulations including the most abundant ionization stages rather than only two ions.

4. Synthetic spectra

The product $n_0 v$ varies between about 2.3×10^{16} to $2 \times 10^{17} \text{ cm}^{-2} \text{ s}^{-1}$ for a 0.87 MeV H heating beam and 100 keV H diagnostic beam, respectively, assuming the cross sectional area of the beam to be 5000 cm^2 . For simplicity, the CR simulations below are performed at $n_0 v = 10^{17} \text{ cm}^{-2} \text{ s}^{-1}$. In the following discussion, we split a wide spectral range of 0.1–1000 nm into four intervals, namely, 0.1–1, 1–10, 10–100, and 100–1000 nm.

The shortest-wavelength range of 0.1–1 nm contains spectral lines due to the 3–4, 3–5 and other $\Delta n > 0$ transitions including the inner-shell 2–3 transitions. The relative intensities of these spectral lines are only slightly affected by the charge exchange recombination although there is some minimal enhancement of $3d-4f$ and $4f-5g$ lines due to cascades from higher states. Next, the 1–10 nm spectral range is dominated by the D-doublet $3s_{1/2}-3p_{1/2}$ and $3s_{1/2}-3p_{3/2}$ [32] transitions that show practically no variation in relative line intensities with or without charge exchange. This is due to the fact that on the one hand, the upper levels $3p$ are very strongly populated by the direct excitation from the ground state, and on the other hand, the CX population flux into the high- n states does not seem to affect the *relative* population of the $j = 1/2$ and $j = 3/2$ levels of the $3p$ configuration.

The CX effect on spectral line intensities becomes very pronounced for the VUV, UV, and visible part of the spectra. Figure 7 presents comparison of the VUV spectra between 10

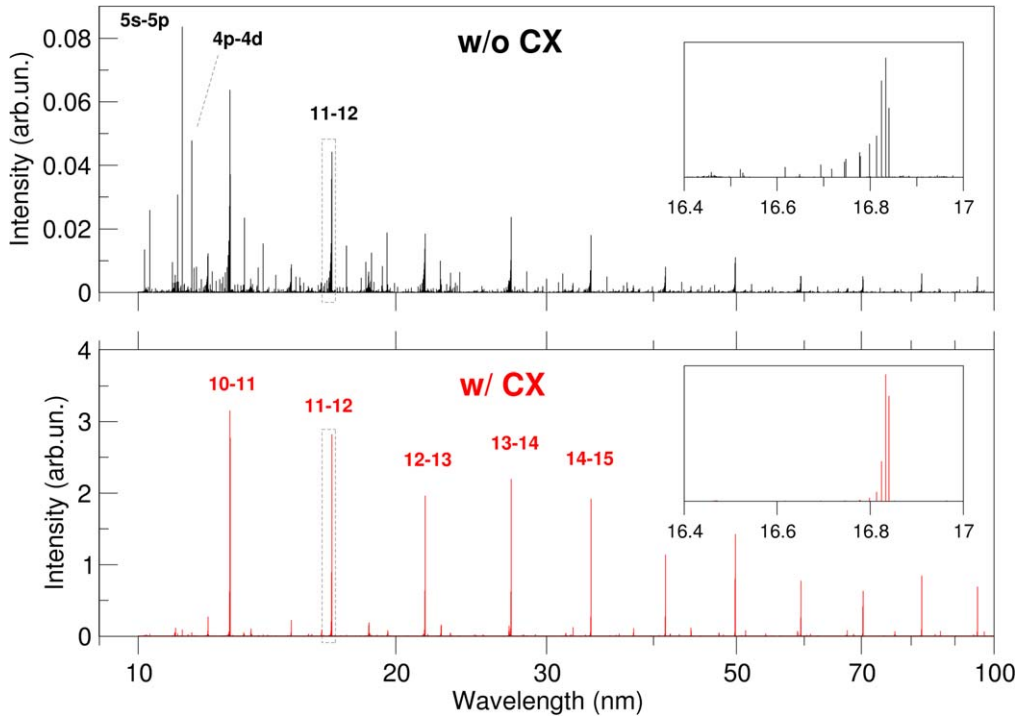


Figure 7. Comparison of VUV spectra for an ITER-type plasma at the beam energy of 500 keV/u without CX (top) and with pCTMC CX at $n_0v = 10^{17} \text{ cm}^{-2} \text{ s}^{-1}$ (bottom). Insets show the spectrum features near the 11–12 spectral transitions. Note the significantly different intensity scales of the two graphs with and without consideration of the CX.

and 100 nm, without (top) and with (bottom) charge exchange included via data from the pCTMC model at $E_B = 500 \text{ keV/u}$. Without CX, the strongest line in this spectral range is the $5s_{1/2}-5p_{3/2}$ transition at 11.26 nm, with the nearby relatively intense $4p_{3/2}-4d_{5/2}$ line at 11.55 nm. A series of strong lines with decreasing intensity correspond to the $\Delta n = 1$, $|\Delta l| = 1$ transitions: 10–11 at 12.80 nm, 11–12 at 16.83 nm, 12–13 at 21.64 nm, and so on. The spectrum also contains a large number of less intense lines, some of which have the same initial and final n values as above (for instance, $11s-12p$ at 14.48 nm) and some of which correspond to very different combinations of n 's. The inset shows the line intensity distribution between 16.4 and 17.0 nm. Here the spectral lines at $\lambda < 16.6 \text{ nm}$ are primarily due to the 15–18 transitions while at longer wavelengths the $11l-12l'$ manifold dominates. Note that the strongest lines in this manifold are due to E1 transitions between levels with high values of l and $l \pm 1$ that are primarily populated by radiative cascades from higher states.

Introduction of charge exchange completely changes the spectral picture (figure 7, bottom). The $\Delta n = 0$ transitions become almost negligible compared to the $\Delta n = 1$ transitions. Moreover, the intensity distribution within the $\Delta n = 0$ manifold is strongly modified as well, becoming even more sharply clustered near the $11l-12l'$ transitions with the highest possible values of l and l' . This seems to contradict the l -distribution of CX cross sections (figure 5) for relatively low values of principal quantum numbers that have parabolic shape without any preference for high- l values. However, the CX cross sections for $n \sim 11-12$ are several orders of magnitude smaller than those into the states with $n \sim n_{\text{max}}$. As was mentioned above (see figure 5), for those states the CX

distribution is strongly tilted towards the highest- l states that cannot radiatively decay into lower states with $\Delta n > 1$. Therefore, the radiative cascades from the CX-populated nl states proceed along the states with the highest values of orbital angular momentum. This also explains the enhancement of the $3d-4f$ and $4f-5g$ lines in the 0.1–1 nm spectral range. Note also that for the longer wavelength range from 100 to 1000 nm (figure 8) the CX effects are similar to the ones observed for the (10–100) nm range of figure 7.

An important question is whether some features of the experimental spectra can be used to distinguish between the different theoretical methods. Figure 9 presents comparisons of the rCTMC and pCTMC spectra in the 100–1000 nm range calculated at 100keV/u (top) and 500 keV/u (bottom). The spectra are normalized to the strongest line and for better visibility the pCTMC spectra (in red) are shifted to longer wavelengths by 3 nm. While the 500 keV/u spectra look very similar for both methods, the 100 keV/u spectra show clear dissimilarity above 350 nm where the $\Delta n = 1$ transitions for high $n > 30$ are located. Therefore, the ratio of the line intensities above, say, 300–400 nm to the strongest lines should provide a strong indication as to which method better explains the experimental data. The explanation certainly is obvious from the already discussed difference in the rCTMC and pCTMC cross sections (figures 3 and 4).

5. Summary

Use of energetic neutral beams for heating and diagnostics of magnetic fusion plasmas inevitably involves simulations of

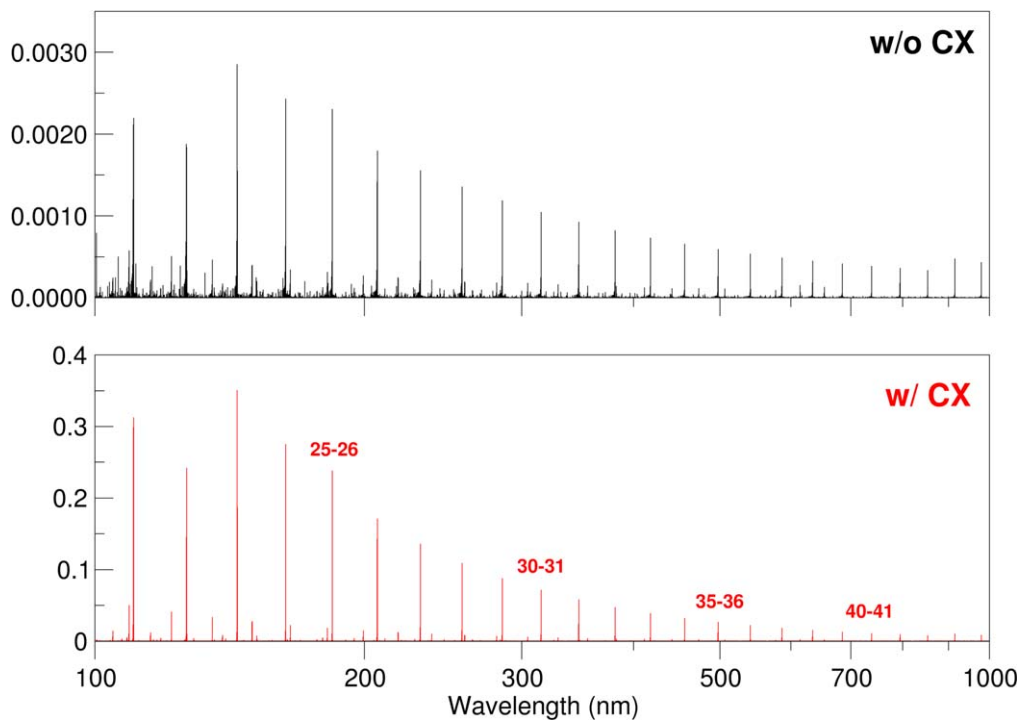


Figure 8. Same as figure 7 for the 100–1000 nm range.

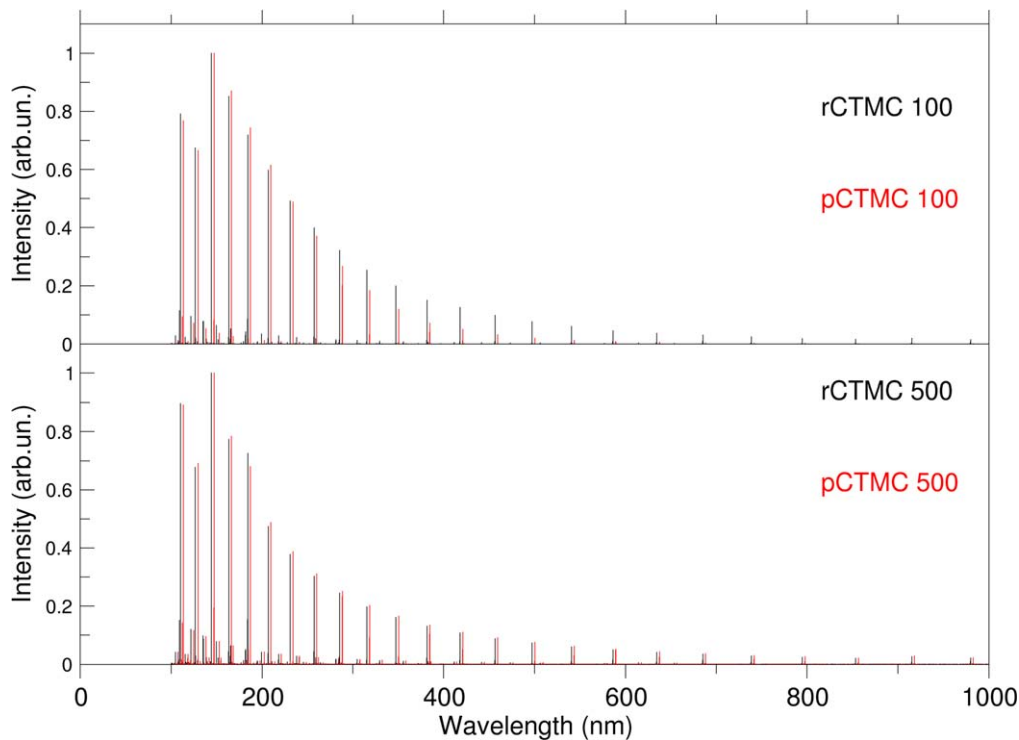


Figure 9. Comparison of normalized spectra using either rCTMC and pCTMC CX calculations for 100 keV/u (top) and 500 keV/u (bottom). For better visibility the pCTMC spectra (in red) are shifted by +3 nm.

plasma emission due to their interactions with other particles. Since tungsten is expected to be one of the major impurities for ITER, it is paramount to reach an adequate understanding of its spectra from charge exchange with the neutral particles. This has to include both accurate calculation of the elementary interactions between W ions and H/D atoms and correct

modeling of the resulting spectra. The present work addresses a more readily achieved first approximation including just the most abundant tungsten ion, W^{6+} , of the ITER plasma. Even within such a limited approach we have shown that the account charge exchange leads to noticeable modification of the spectrum, particularly in the visible range. It is found that

intensities of $\Delta n = 1$ lines are strongly altered and thus can be used to quantify the CX effect on level populations and resulting spectra. A future publication will report a more realistic multi-ion calculation of CX spectra for typical ITER conditions.

ORCID iDs

Yu Ralchenko  <https://orcid.org/0000-0003-0083-9554>

References

- [1] Groebner R J, Brooks N H, Burrell K H and Rottler L 1983 *Appl. Phys. Lett.* **43** 920
- [2] Isler R C 1987 *Phys. Scr.* **35** 650
- [3] Boileau A, von Hellermann M G, HJorton L D, Spence J and Summers H P 1989 *Plasma Phys. Control. Fusion* **31** 779
- [4] Marchuk O, Ralchenko Y, Janev R K, Bershinger G and Biel W 2009 *J. Phys. B* **42** 165701
- [5] Progress in the ITER Physics Basis 2007 *Nucl. Fus.* **47** S1–414
- [6] Schultz D R, Lee T-G and Loch S D 2010 *J. Phys. B* **43** 144002
- [7] Schlummer T, Marchuk O, Schultz D R, Bertschinger G, Biel W, Reiter D and the TEXTOR-Team 2015 *J. Phys. B* **48** 144033
- [8] Olson R E 1981 *Phys. Rev. A* **24** 1726
- [9] Janev R K, Presnyakov L P and Shevelko V P 1985 General features of single-charge-transfer cross sections *Physics of Highly Charged Ions* (Berlin: Springer) ch 7
- [10] Abrines R and Percival I C 1966 *Proc. Phys. Soc.* **88** 861
- [11] Olson R E and Salop A 1977 *Phys. Rev. A* **16** 531
- [12] Becker R L and MacKellar A D 1984 *J. Phys. B* **17** 3923
- [13] Olson R E and Schultz D R 1989 *Phys. Scr.* **T28** 71
- [14] Schultz D R, Meng L, Reinhold C O and Olson R E 1991 *Phys. Scr.* **T37** 89
- [15] Minami T, Pindzola M S, Lee T-G and Schultz D R 2006 *J. Phys. B* **39** 2877
- [16] Schultz D R and Krstic P S 1995 *At. Plasma-Mater. Interact. Data Fusion* **6** 173
- [17] Schultz D R, Krstic P S and Reinhold C O 1996 *Phys. Scr.* **T62** 69
- [18] Minami T, Lee T-G, Pindzola M S and Schultz D R 2008 *J. Phys. B* **41** 135201
- [19] Hardie D J W and Olson R E 1983 *J. Phys. B* **16** 1983
- [20] Cohen J S 1985 *J. Phys. B* **18** 1759
- [21] Cariatore N D, Otranto S and Olson R E 2015 *Phys. Rev. A* **91** 042709
- [22] Whyte D G, Isler R C, Wade M R, Schultz D R, Krstic P S, Hung C C and West W P 1998 *Phys. Plasmas* **5** 3694
- [23] Fritsch W and Lin C D 1991 *Phys. Rep.* **202** 1
- [24] Errea L F, Illescas C, Mendez L, Pons B, Riera A and Suarez J 2006 *J. Phys. B* **39** L91
- [25] Dz B, Gayet R and Salin A 1984 *Comput. Phys. Commun.* **32** 385
- [26] Ralchenko Yu *et al* 2009 16th Int. Conf. on Atomic Processes in Plasmas *AIP Proceedings* **1161** 242
- [27] Sobelman I I, Vainshtein L A and Yukov E A 1995 *Excitation of Atoms and Broadening of Spectral Lines* (Berlin: Springer)
- [28] Ralchenko Yu (ed) 2016 *Modern Methods in Collisional-Radiative Modeling of Plasmas* (Berlin: Springer)
- [29] Ralchenko Yu V and Maron I 2001 *J. Quant. Spectr. Rad. Transfer* **71** 609
- [30] Gu M F 2011 *Can. J. Phys.* **86** 675
- [31] Marchuk O, Ralchenko Yu and Schultz D R 2012 *Plasma Phys. Control. Fusion* **54** 095010
- [32] Gillaspay J D, Draganić I N, Ralchenko Yu, Reader J, Tan J N, Pomeroy J M and Brewer S M 2009 *Phys. Rev. A* **80** 010501